universe

MDPI

Communication

First Results of the ^{140}Ce(n,γ)^{141}Ce Cross-Section Measurement at n_TOF

Simone Amaducci [1,2,*], Nicola Colonna [3], Luigi Cosentino [1], Sergio Cristallo [4,5], Paolo Finocchiaro [1], Milan Krtička [6], Cristian Massimi [7,8], Mario Mastromarco [9], Annamaria Mazzone [3,10], Alberto Mengoni [11], Stanislav Valenta [6], Oliver Aberle [9], Victor Alcayne [12], Józef Andrzejewski [13], Laurent Audouin [14], Victor Babiano-Suarez [15], Michael Bacak [9,16,17], Massimo Barbagallo [3,9], Samuel Bennett [18], Eric Berthoumieux [17], Jon Billowes [18], Damir Bosnar [19], Adam Brown [20], Maurizio Busso [4,21], Manuel Caamaño [22], Luis Caballero-Ontanaya [15], Francisco Calviño [23], Marco Calviani [9], Daniel Cano-Ott [12], Adria Casanovas [23], Francesco Cerutti [9], Enrico Chiaveri [9,18], Guillem Cortés [23], Miguel Cortés-Giraldo [24], Lucia-Anna Damone [3,25], Paul-John Davies [18], Maria Diakaki [9,26], Mirco Dietz [27], Cesar Domingo-Pardo [15], Rugard Dressler [28], Quentin Ducasse [29], Emmeric Dupont [17], Ignacio Durán [22], Zinovia Eleme [30], Beatriz Fernández-Domínguez [22], Alfredo Ferrari [9], Valter Furman [31], Kathrin Göbel [32], Ruchi Garg [27], Aleksandra Gawlik [13], Simone Gilardoni [9], Isabel Gonçalves [33], Enrique González-Romero [12], Carlos Guerrero [24], Frank Gunsing [17], Hideo Harada [34], Stephan Heinitz [28], Jan Heyse [35], David Jenkins [20], Arnd Junghans [36], Franz Käppeler [37], Yacine Kadi [9], Atsushi Kimura [34], Ingrid Knapova [11], Michael Kokkoris [26], Yuri Kopatch [31], Deniz Kurtulgil [32], Ion Ladarescu [15], Claudia Lederer-Woods [27], Helmut Leeb [16], Jorge Lerendegui-Marco [24], Sarah-Jane Lonsdale [27], Daniela Macina [9], Alice Manna [7,8], Trinitario Martínez [12], Alessandro Masi [9], Pierfrancesco Mastinu [38], Emilio-Andrea Maugeri [28], Emilio Mendoza [12], Veatriki Michalopoulou [9,26], Paolo Milazzo [39], Federica Mingrone [9], Javier Moreno-Soto [17], Agatino Musumarra [1,40], Alexandru Negret [41], Francisco Ogállar [42], Andreea Oprea [41], Nikolas Patronis [30], Andreas Pavlik [43], Jarosław Perkowski [13], Luciano Piersanti [4,5], Cristina Petrone [41], Elisa Pirovano [29], Ignacio Porras [42], Javier Praena [42], José-Manuel Quesada [24], Diego Ramos-Doval [14], Thomas Rauscher [44,45], René Reifarth [32], Dimitri Rochman [28], Carlo Rubbia [9], Marta Sabaté-Gilarte [9,24], Alok Saxena [46], Peter Schillebeeckx [35], Dorothea Schumann [28], Adhitya Sekhar [18], Gavin Smith [18], Nikolay Sosnin [18], Peter Sprung [28], Athanasios Stamatopoulos [26], Giuseppe Tagliente [3], José Tain [15], Ariel Tarifeño-Saldivia [23], Laurent Tassan-Got [9,26,14], Benedikt Thomas [32], Pablo Torres-Sánchez [42], Andrea Tsinganis [9], Jiri Ulrich [28], Sebastian Urlass [9,36], Gianni Vannini [7,8], Vincenzo Variale [3], Pedro Vaz [33], Alberto Ventura [7], Diego Vescovi [4,5,47], Vasilis Vlachoudis [9], Rosa Vlastou [26], Anton Wallner [48], PhilipJohn Woods [27], Tobias Wright [18], Petar Žugec [19] and on behalf of the n_TOF Collaboration

1 INFN Laboratori Nazionali del Sud, 95125 Catania, Italy
2 Dipartimento di Fisica e Astronomia, Università di Catania, 2, 95131 Catania, Italy
3 Istituto Nazionale di Fisica Nucleare, Sezione di Bari, 70126 Bari, Italy
4 Istituto Nazionale di Fisica Nucleare, Sezione di Perugia, 06123 Perugia, Italy
5 Istituto Nazionale di Astrofisica—Osservatorio Astronomico d'Abruzzo, 64100 Collurania, Italy
6 Charles University, 11000 Prague, Czech Republic
7 Istituto Nazionale di Fisica Nucleare, Sezione di Bologna, 40127 Bologna, Italy
8 Dipartimento di Fisica e Astronomia, Università di Bologna, 40129 Bologna, Italy
9 European Organization for Nuclear Research (CERN), 1211 Geneva, Switzerland
10 Consiglio Nazionale delle Ricerche, 7, 00185 Bari, Italy
11 Agenzia Nazionale per le Nuove Tecnologie (ENEA), 40129 Bologna, Italy
12 Centro de Investigaciones Energéticas Medioambientales y Tecnológicas (CIEMAT), 28040 Madrid, Spain
13 University of Lodz, 90-137 Łódź, Poland
14 Institut de Physique Nucléaire, CNRS-IN2P3, University Paris-Sud, Université Paris-Saclay, CEDEX, F-91406 Orsay, France
15 Instituto de Física Corpuscular, CSIC—Universidad de Valencia, 46980 Paterna, Spain
16 Technische Universität Wien, 1040 Vienna, Austria
17 CEA Irfu, Université Paris-Saclay, F-91191 Gif-sur-Yvette, France
18 University of Manchester, Manchester M13 9PL, UK
19 Department of Physics, Faculty of Science, University of Zagreb, 10000 Zagreb, Croatia
20 University of York, York YO10 5DD, UK
21 Dipartimento di Fisica e Geologia, Università di Perugia, 06123 Perugia PG, Italy
22 University of Santiago de Compostela, Santiago de Compostela, 15705 Compostela, Spain
23 Universitat Politècnica de Catalunya, 08034 Barcelona, Spain
24 Universidad de Sevilla, 41004 Sevilla, Spain

Citation: Amaducci, S.; Colonna, N.; Cosentino, L.; Cristallo, S.; Finocchiaro, P.; Krtička, M.; Massimi, C.; Mastromarco, M.; Mazzone, A.; Mengoni, A.; et al. First Results of the ^{140}Ce(n,γ)^{141}Ce Cross-Section Measurement at n_TOF. *Universe* **2021**, *7*, 200. https://doi.org/10.3390/universe7060200

Academic Editors: Sergio Cristallo and Paolo Ventura

Received: 31 March 2021
Accepted: 17 May 2021
Published: 17 June 2021

[25] Dipartimento di Fisica, Università degli Studi di Bari, 70121 Bari, Italy
[26] National Technical University of Athens, Athens, 10682, Greece
[27] School of Physics and Astronomy, University of Edinburgh, Edinburgh EH9 3FD, UK
[28] Paul Scherrer Institut (PSI), 5232 Villingen, Switzerland
[29] Physikalisch-Technische Bundesanstalt (PTB), Bundesallee 100, 38116 Braunschweig, Germany
[30] University of Ioannina, 451 10 Ioannina, Greece
[31] Joint Institute for Nuclear Research (JINR), 141980 Dubna, Russia
[32] Goethe University Frankfurt, 60323 Frankfurt am Main, Germany
[33] Instituto Superior Técnico, 1049-001 Lisbon, Portugal
[34] Japan Atomic Energy Agency (JAEA), Tokai-mura 319-1184, Japan
[35] European Commission, Joint Research Centre, Geel, Retieseweg 111, B-2440 Geel, Belgium
[36] Helmholtz-Zentrum Dresden-Rossendorf, 01328 Dresden, Germany
[37] Karlsruhe Institute of Technology, Campus North, IKP, 76021 Karlsruhe, Germany
[38] Istituto Nazionale di Fisica Nucleare, Sezione di Legnaro, 35020 Legnaro, Italy
[39] Istituto Nazionale di Fisica Nucleare, Sezione di Trieste, 34149 Trieste, Italy
[40] Dipartimento di Fisica e Astronomia, Università di Catania, 95123 Catania, Italy
[41] Horia Hulubei National Institute of Physics and Nuclear Engineering, P.O. Box MG-6, RO-76900 Bucharest, Romania
[42] University of Granada, 18010 Granada, Spain
[43] Faculty of Physics, University of Vienna, 1090 Vienna, Austria
[44] Department of Physics, University of Basel, CH-4056 Basel, Switzerland
[45] Centre for Astrophysics Research, University of Hertfordshire, Herts AL10 9AB, UK
[46] Bhabha Atomic Research Centre (BARC), Maharashtra 400094, India
[47] Gran Sasso Science Institute, 67100 L'Aquila, Italy
[48] Australian National University, 2600 Canberra, Australia
* Correspondence: amaducci@lns.infn.it; Tel.: +39-3387997513

Abstract: An accurate measurement of the ^{140}Ce(n,γ) energy-dependent cross-section was performed at the n_TOF facility at CERN. This cross-section is of great importance because it represents a bottleneck for the s-process nucleosynthesis and determines to a large extent the cerium abundance in stars. The measurement was motivated by the significant difference between the cerium abundance measured in globular clusters and the value predicted by theoretical stellar models. This discrepancy can be ascribed to an overestimation of the ^{140}Ce capture cross-section due to a lack of accurate nuclear data. For this measurement, we used a sample of cerium oxide enriched in ^{140}Ce to 99.4%. The experimental apparatus consisted of four deuterated benzene liquid scintillator detectors, which allowed us to overcome the difficulties present in the previous measurements, thanks to their very low neutron sensitivity. The accurate analysis of the p-wave resonances and the calculation of their average parameters are fundamental to improve the evaluation of the ^{140}Ce Maxwellian-averaged cross-section.

Keywords: cerium; ^{140}Ce; neutron; capture; cross-section; s-process; n_TOF; MACS; nucleosynthesis

1. Introduction

It has been well ascertained since the late 1950s that the vast majority of the elements above the iron peak are synthesized in stars, via sequences of neutron captures and β-decays [1,2]. Depending on the typical time elapsing between two consecutive neutron captures, and hence on the available neutron densities, these processes are referred to as slow (s) or rapid (r). In the r-process, neutron densities as high as 10^{18}–10^{22} cm^{-3} are attained, triggering the production of very neutron-rich nuclei in an extremely short time, by means of neutron capture sequences much faster than the β-decays. The physical conditions of the r-process are met in explosive scenarios, such as neutron star mergers or core-collapse supernovae, which have typical time scales of the order of a few seconds. The s-process mainly takes place in the late evolutionary phases of low-mass stars, in particular during their thermally pulsing asymptotic giant branch (TP-AGB) phase. During that evolutionary stage, a succession of burning and mixing episodes leads to the production of neutrons through the reactions ^{13}C(α,n)^{16}O and ^{22}Ne(α,n)^{25}Mg. While the former reaction

is the major neutron source in low-mass AGBs, the latter significantly contributes to heavy-element nucleosynthesis in more massive AGBs (5–6 M_{sun}) (see, e.g., [3,4]). Typical neutron densities in AGB stars are $\approx 10^7$ cm^{-3}: the relatively long time between two consecutive captures allows the unstable nuclei to eventually β-decay; the resulting s-process path then follows the valley of stability up to the synthesis of lead and bismuth.

In the last few decades, accurate knowledge of the s-process site led to a considerable effort in modeling the evolution of the AGB stars and evaluating the contribution of all the nuclear reactions involved in the nucleosynthesis of heavy elements (see, e.g., [5–8]). These models allowed studying the AGB chemical evolution and their role as polluters of the galactic medium. Clearly, high-quality nuclear data are required in order to determine the final abundances of all the elements produced in stellar interiors. This holds in particular for neutron capture cross-sections. The comparison between the observed abundances and the ones predicted by stellar models represents an essential tool to test the robustness of the models, in particular for those elements that are synthesized mainly via the s-process.

Such a kind of comparison was carried out by Straniero et al. [9], considering the globular clusters M4 [10] and M22 [11]. Thanks to the presence of many stars, which allow calculating the average distributions and the clear determination of the r-process contribution, these clusters represent an ideal site to test the robustness of s-process predictions. Figure 1 shows the comparison between stellar models' predictions and the chemical composition of M22 stars, in the usual spectroscopic notation[1]. In this case, AGB stars in the mass range 3–6 M_{sun} contribute to the s-process production. In general, a good agreement is observed for most of the elements, but a large discrepancy is present in the case of Ce (Z = 58). For cerium, belonging to the second s-process peak (Ba-La-Pr-Nd), the theoretical expectation is ≈30% lower than the values observed in the M22 cluster, while nearby elements astonishingly agree with the theory. Being a neutron-magic nucleus, ^{140}Ce represents a very interesting isotope, since its very small capture cross-section acts as a bottleneck for the s-process, greatly enhancing its abundance with respect to the nearby non-magic isotopes. Since the majority of natural cerium is made of ^{140}Ce (89%), its destruction channel, i.e., the capture of a neutron, largely determines the cerium abundance on the stellar surface. The reaction ^{140}Ce(n,γ) lacks accurate experimental data, while its production channel, the neutron capture on ^{139}La, has already been investigated with high accuracy at n_TOF [12]. Therefore, a nuclear origin of the discrepancy needed to be further investigated, since a reduction of the ^{140}Ce(n,γ) cross-section could justify the observed overestimation. Considering the potential contributions from AGBs with different initial masses, the evaluation of a variation of the neutron capture rate on the whole energy spectrum will be performed when the stellar neutron capture rate is available.

The main nuclear capture quantities that serve as the input for s-process nucleosynthesis models are the MACS, i.e., the convolution of the capture cross-sections and the Maxwellian energy distribution of neutrons for a given temperature kT. The results presented in [9] were obtained by using the MACS provided by the database KADoNiS0.3 [13], which is a (on-line) database for cross-sections relevant to the s- and p-processes. The MACS reported in KADoNiS comes from activation measurement [14] of a natural cerium sample using a quasi-stellar neutron spectrum of kT = 25 keV. Theoretical models, based on the Hauser–Feshbach (HF) theory, permitted extrapolating the experimental MACS for other values of kT. The HF calculations of the 30 keV MACS reported in [14] overestimated the experimental MACS by 30% in the case of ^{140}Ce. The disagreement is related to the uncertainty and incorrectness of the average resonance parameters used in the calculations. Although there exist estimates based on experimental data of resonance spacing (D_0) and radiation width (Γ_γ) for s-wave resonances, any estimate of the average Γ_γ for p-wave (and higher l) resonances is missing (and is thus based only on calculations). Furthermore, since the large part of the ^{140}Ce captures take place at kT ≈ 8 keV, its abundance results in being even more sensitive to the extrapolation of the MACS towards lower energies, especially because relatively few resonances are present in this energy range.

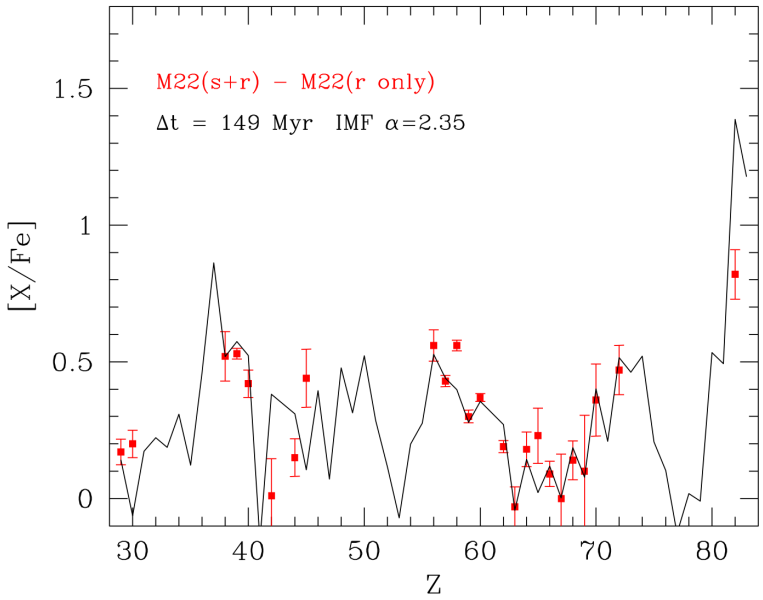

Figure 1. Average abundances observed in the globular cluster M22 (red points) compared to the theoretical expectations deduced from stellar models (from [9]).

Very few experimental energy-dependent cross-sections of ^{140}Ce are available, and the cross-section reported by the nuclear libraries largely relies on transmission experiments, usually performed with natural cerium samples, hence with large effects due to the presence of ^{142}Ce (which acts as a contaminant). The only capture measurement with an energy resolution sufficient to effectively resolve individual resonance was performed by Musgrove et al. [15], where C_6F_6 detectors were employed, which are known to be not particularly suited for capture measurement on isotopes with very high scattering cross-sections [16], such as ^{140}Ce.

The lack of highly reliable experimental data makes the evaluation process very challenging, so that it is not surprising that the MACS evaluated with the resonance parameters of the major nuclear libraries (as ENDF, JEFF, and JENDL) led to very different results, as shown in Figure 2. In particular, the MACS calculated with the ENDF/B-VIII [17], JENDL-4.0 [18], and JEFF3.3 [19] resonance parameters largely disagree, and all are systematically lower than KADoNiS0.3 and the most recent KADoNiS1.0 [20]. The accuracy of the MACS can be significantly improved by adding new experimental data. In particular, more strict constraints on the statistical model parameters are required to reduce the uncertainty of the theoretical calculations. In order to clarify the discrepancy that emerged in [9] and to produce a more accurate evaluation of the MACS, a new measurement of the ^{140}Ce(n,γ) cross-section was performed at the n_TOF facility in 2018.

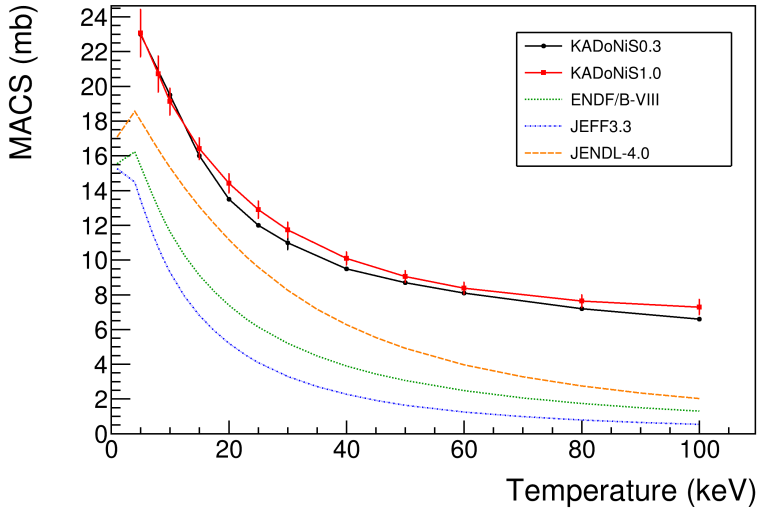

Figure 2. The MACS calculated with the resonance parameters provided by major libraries compared with the values reported in KADoNiS0.3 and KADoNiS1.0.

2. Experimental Apparatus and Data Analysis

The n_TOF facility represents a unique site where high-precision measurements of neutron-induced cross-sections can be performed. Since its operational start in 2001, the n_TOF collaboration [21] has largely contributed to the improvement of nuclear data of interest for the nuclear astrophysics community, in particular performing many accurate neutron capture cross-section measurements (see, e.g., the two recent works [22,23]). The n_TOF white pulsed neutron beam is produced by spallation reactions on a cylindrical lead target induced by a 20 GeV/c proton beam accelerated with the CERN Proton Synchrotron (PS). The kinetic energy of the neutrons reaching the two experimental areas is measured with the time-of-flight technique. The ^{140}Ce(n,γ) measurement required the high-energy resolution of the beam present in Experimental Area 1 (EAR1), thanks to its long flight path of ≈185 m. In EAR1, it is possible to reach a resolution from 5×10^{-4} at 1 keV to 3×10^{-3} at 100 keV [24], which is essential to effectively resolve the resonances in the region of interest.

The sample employed was composed of 12.318 grams of CeO_2 powder, enriched to 99.4% of ^{140}Ce, with only 0.6% of ^{142}Ce as a relevant contamination (natural cerium presents 11% of ^{142}Ce). The sample was produced at Paul Sherrer Insitut (PSI) via the sintering process. The CeO_2 powder was pressed and enclosed in a PEEK (polyether ether ketone) cylindrical capsule of 1 mm in thickness and heated at 100 °C for 4 h in a glove box with a controlled O_2 and H_2O atmosphere (concentration lower than 1 ppm). A ^{197}Au sample, having a diameter almost identical to the cerium one, was used to normalize the cerium data and to exactly determine the flight path length. The latter was obtained from fitting the gold capture resonances in the energy interval from 100 eV to 2 keV. In order to evaluate the different sources of background data, an empty sample was used to measure the component related to the beam, while a lead sample was employed to measure the sample-related background. Finally, the detectors were calibrated, acquiring data on a weekly basis with four γ sources: ^{137}Cs, ^{137}Y, Am-Be, and Cm-C.

The neutron captures were observed by detecting the γ-rays produced by the decay of the compound nucleus ^{141}Ce. The experimental apparatus was made of four deuterated benzene (C_6D_6) liquid scintillator detectors [25] encapsulated in a cylindrical case made of carbon fiber, to guarantee a very low neutron sensitivity. A relatively high neutron sensitivity is one of the difficulties encountered with C_6F_6 detectors employed in the measurement by [15]. The detectors were placed at ≈10 cm from the center of the sample holder at angles of 125° with respect to the neutron beam. The adopted configuration minimized the effect of the anisotropic emission of γ-rays; moreover, the upstream position

with respect to the sample position reduced the background due to the in-beam γ-rays, which were scattered by the sample. In order to monitor the neutron flux, the Silicon Monitor (SiMon) detector [26] was installed upstream with respect to the capture apparatus.

The data analysis employed the total energy detection principle in combination with the pulse height weighting technique [27,28] to eliminate the dependence of the detection efficiency from the γ cascade path following the neutron capture. This is achieved if the detection efficiency of an i-th γ ray, emitted during the γ cascade, is proportional to its energy E_γ^i. In such a case, the detection of the full cascade becomes proportional to its total energy E_γ^{tot}:

$$\varepsilon_{cascade} = \sum_{i=1}^{m} \varepsilon_i(E_\gamma^i) = \sum_{i=1}^{m} k \times E_\gamma^i = k \times E_\gamma^{tot} \quad (1)$$

In the case of C_6D_6 detectors, the proportionality between the deposited energy and the γ-rays detection efficiency is achieved through an off-line weighting function applied to the detector signals. These functions were calculated by simulating the full experimental apparatus with a Monte Carlo simulation, performed with the Geant4 [29] code. After the weighting procedure, the experimental capture yield can be written as:

$$Y_{exp}(E_n) = N \frac{C_w(E_n) - B_w(E_n)}{\varepsilon(E_n)\phi(E_n)} \quad (2)$$

where C_w are the weighted count rates with the sample, B_w is the weighted background, ϕ the neutron flux on the target, and N a normalization factor. The latter includes many geometrical factors, such as the sample area, the beam interception factor (BIF), and the different solid angle of the flux monitor and the capture setup. The neutron flux measured with SiMon was compared with the official n_TOF flux [30], evaluated with different detectors and standard reactions, resulting in an excellent agreement in the energy interval of interest. Therefore, in order to calculate the ^{140}Ce capture yield, the official neutron flux was used, which is known with an uncertainty better than 1% below 3 keV and within 4–5% up to 100 keV.

The gold sample background was evaluated according to the method described in [28], using the data collected with the empty sample and with the lead sample, properly scaled. As an example, Figure 3 shows the gold neutron energy spectrum for one of the detectors, compared with the background and the beam-off component. The latter corresponds to the ambient background, and it is almost negligible for $E_n > 10$ eV. As expected, from 20 to 50 eV, the gold spectrum is almost equal to the background because of the very small ^{197}Au capture cross-section, confirming the correctness of the procedure adopted for the background evaluation. The same method could not be applied for cerium, since the component of the background depending on the sample was dominant, due to the very high areal density of the cerium sample (1.291×10^{-2} atoms/barn) and high neutron scattering cross-section. At the present stage of analysis, the cerium background is considered to be linear in the vicinity of each fitted resonance. A more rigorous approach, by means of a Monte Carlo simulation, is currently under study.

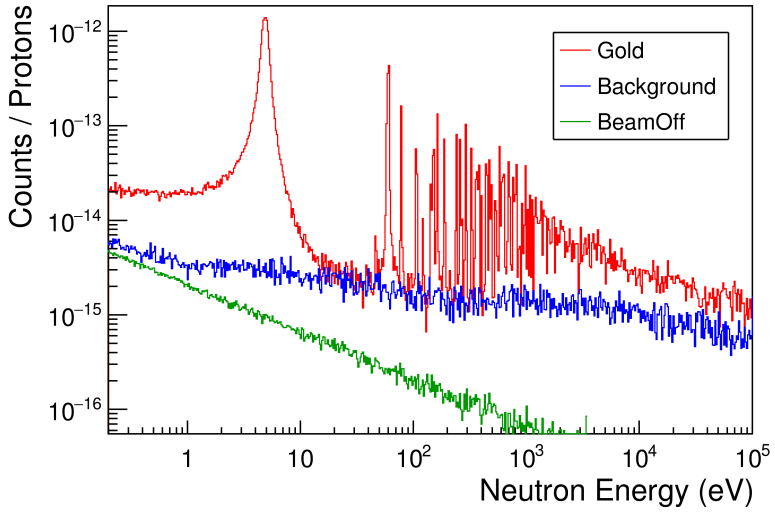

Figure 3. Energy spectrum measured with the gold sample (red), compared with the total evaluated background (blue) and the ambient background (green).

The normalization factor N was calculated by applying the saturated resonance method [31] to the opaque gold capture resonance at 4.9 eV. The resulting value (N = 0.7127 ± 0.0014) was substantially in agreement with the beam interception factor reported in [24] for the 2 cm-diameter samples. The cerium data were suitably corrected to take into account the slightly smaller diameter of the sample (1.95 cm). The gold data allowed verifying the robustness of the analysis in the energy interval where the ^{140}Ce capture resonances are located. Figure 4 shows that the experimental results on average agreed with the ^{197}Au(n,γ) cross-section evaluated by the ENDF/B-VIII library, in the neutron energy range from 1 keV to 100 keV.

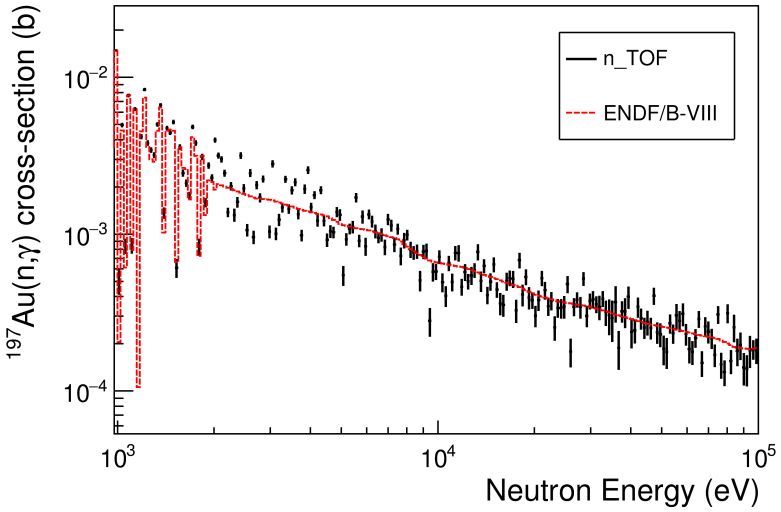

Figure 4. Experimental ^{197}Au(n,γ) cross-section (black dots) compared to the evaluation of ENDF/B-VIII (red dashed line).

A preliminary analysis of the cerium capture yield was carried out with the Bayesian R-matrix code SAMMY [32]. This code can manage the self-shielding and multiple interactions of neutrons in the sample and other experimental effects such as Doppler and resolution broadening by including the resolution function, which is a property of all neutron time-of-flight facilities, which describes the distribution of the neutron time of flight for a given kinetic energy. The resonance parameters provided by the JENDL-4.0

library were initially adopted as a reference, including the spin-parity assignment, which was almost identical to those of other libraries, such as ENDF/B-VIII.

3. Discussion and perspectives

The preliminary ^{140}Ce data allowed resolving and performing the resonance shape analysis (RSA) of 81 of the 102 resonances reported by the library JENDL-4.0 below 65 keV, to determine their kernel[2] and in some cases the radiation and scattering widths (Γ_γ and Γ_n, respectively). Between 2.5 keV, where the first ^{140}Ce resonance is located, and 34 keV, the data made it possible to fit the parameters of 46 resonances, while JENDL-4.0 reported 47 resonances. From 34 keV to 65 keV, JENDL-4.0 indicated the presence of 55 resonance, while the experimental data allowed fitting 35 of them; no resonances could be clearly identified above. Only one structure due to the ^{142}Ce contamination was observed in the experimental capture yield at 1.15 keV, far away from any ^{140}Ce resonance; hence, the presence of ^{142}Ce did not represent an issue for the analysis.

Figure 5 shows the contribution to the MACS of a different sub-set of resonances using their parameters from the JENDL-4.0 library. It is noteworthy that the resonances with energies lower than 60 keV (red line) made the major contribution to the MACS in the temperature interval of interest for the s-process (<30 keV). One can also observe the importance of the p-waves' contribution, which was responsible for approximately 50% of the MACS at 8 keV and even more with increasing energy. The n_TOF measurement ensured the accurate measurements of the resonances kernel; furthermore, it can increase the accuracy on their average width and spacing with respect to the values available during the evaluation of the MACS by [14].

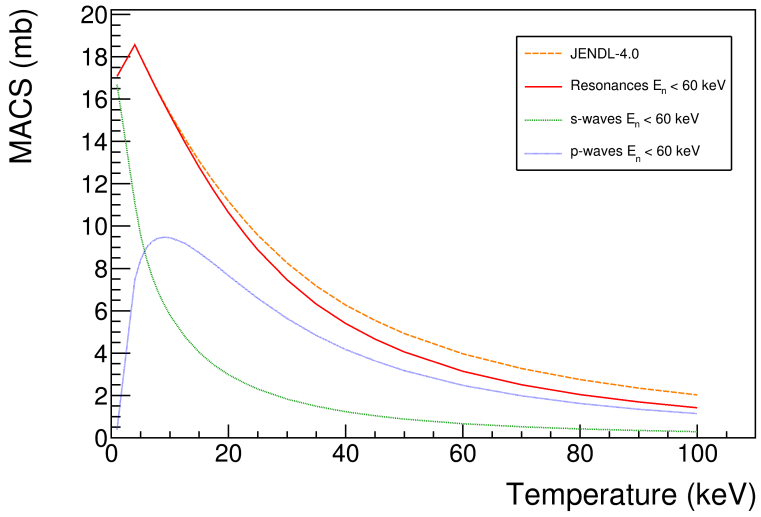

Figure 5. Maxwellian averaged cross-section calculated with the individual resonance parameters as provided by JENDL-4.0 (orange dashed line), compared with the contribution given by different sub-sets of resonances.

An example of the RSA in the case of a p-wave resonance is shown in Figure 6, where the quality of the experimental data is clearly sufficient to accurately determine the kernel and resonance energy. It is interesting that the n_TOF fit of the capture yield showed large discrepancies compared to both the JENDL-4.0 and ENDF/B-VIII libraries. As shown by Table 1, the value of $g\Gamma_\gamma\Gamma_n/\Gamma$ measured at n_TOF was a factor of two larger with respect to both libraries and to the values from [15]. The results showed an excellent energy resolution achievable at n_TOF; in fact, we were able to determine the resonance energy with a precision of two orders of magnitude better than [15].

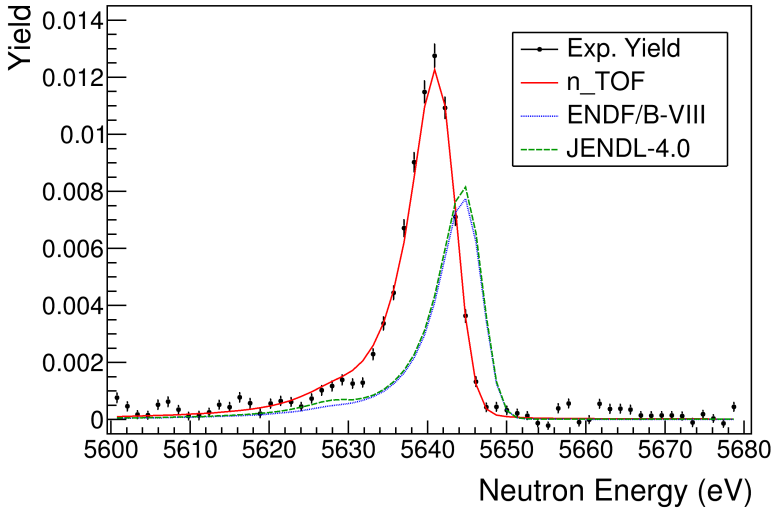

Figure 6. Example of the RSA in the case of p-wave resonance; in this case, the n_TOF fit (red) of the capture yield shows large discrepancies, compared to both the JENDL-4.0 (green) and ENDF/B-VIII (blue) libraries.

Table 1. Capture kernel measured at n_TOF compared to the values reported by the ENDF/B-VIII and JENDL-4.0 libraries and by [15].

Source	Energy (eV)	$g\Gamma_\gamma\Gamma_n/\Gamma$ (meV)
n_TOF	5636.56 ± 0.05	21.6 ± 1.2
JENDL-4.0	5640	11.0
ENDF/B-VIII	5640	10.5
Musgrove et al.	5640 ± 5	10 ± 1

The first results demonstrated that the accurate energy-dependent cross-section of ^{140}Ce(n,γ) was measured successfully at n_TOF and the resonances parameters were determined with uncertainties significantly lower than previous experiments. The combination of the C_6D_6 detectors, with their very low neutron sensitivity, and the high energy resolution of n_TOF were decisive to measure this very low capture cross-section. The data allowed performing a reliable RSA of approximately 80 resonances, a large fraction of which are p-waves. These are of particular interest for the s-process, since they provide a larger contribution to the MACS between 8 keV and 30 keV. Direct experimental information will largely determine the MACS at 8 keV and significantly tighten the constraints of the statistical model to calculate the MACS at about 30 keV. The new neutron capture rate, once included in the nucleosynthesis stellar models, will shed more light on the discrepancy with the cerium abundance measured in the M22 globular cluster.

Author Contributions: Conceptualization, S.C., C.M. and A.M. (Alberto Mengoni); formal analysis, S.A. and A.M. (Annamaria Mazzone); investigation, S.A., L.C., C.M. and A.M. (Alberto Mengoni); supervision, N.C., L.C., S.C., P.F., C.M. and A.M. (Alberto Mengoni); methodology, M.K. and S.V.; writing—original draft, S.A.; writing—review and editing, all the authors; data curation, all the authors. All authors have read and agreed to the published version of the manuscript.

Funding: This research received no external funding.

Acknowledgments: The cerium oxide material for this measurement was provided by T. Katabuchi of the Tokyo Institute of Technology.

Conflicts of Interest: The authors declare no conflict of interest.

Notes

1 $[El/Fe] = \log(N(El)/N(Fe))_{star} - \log(N(El)/N(Fe))_{sun}$.
2 Area of a resonance, defined as $g\Gamma_\gamma\Gamma_n/\Gamma$.

References

1. Burbidge, E.M.; Burbidge, G.R.; Fowler, W.A.; Hoyle, F. Synthesis of the Elements in Stars. *Rev. Mod. Phys.* **1957**, *29*, 547–654. [CrossRef]
2. Cameron, A.G.W. *Stellar evolution, nuclear astrophysics, and nucleogenesis*; PAtomic Energy of Canada Ltd.: Chalk River, ON, Canada, 1957.
3. Busso, M.; Gallino, R.; Wassergurg, G. Nucleosynthesis in Asymptotic Giant Branch Stars: Relevance for Galactic Enrichment and Solar System Formation. *ARA&A* **1999**, *37*, 239.
4. Cristallo, S.; La Cognata, M.; Massimi, C.; Best, A.; Palmerini, S.; Straniero, O.; Trippella, O.; Busso, M.; Ciani, G.F.; Mingrone, F.; et al. The Importance of the $^{13}C(\alpha,n)^{16}O$ Reaction in Asymptotic Giant Branch Stars. *ApJ* **2018**, *859*, 105. [CrossRef]
5. Straniero, O.; Gallino, R.; Cristallo, S. S process in low-mass asymptotic giant branch stars. *Nucl. Phys. A* **2006**, *777*, 311. [CrossRef]
6. Cristallo, S.; Straniero, O.; Gallino, R.; Piersanti, L.; Dominguez, I.; Ledered, M.T. Evolution, Nucleosynthesis, and Yields of Low-mass Asymptotic Giant Branch Stars at Different Metallicities. *ApJ* **2011**, *696*, 797. [CrossRef]
7. Cristallo, S.; Piersanti, L.; Straniero, O.; Gallino, R.; Domínguez, I.; Abia, C.; Di Rico, G.; Quintini, M.; Bisterzo, S. Evolution, Nucleosynthesis, and Yields of Low-mass Asymptotic Giant Branch Stars at Different Metallicities. II. The FRUITY Database. *ApJS* **2011**, *197*, 17. [CrossRef]
8. Cristallo, S.; Straniero, O.; Piersanti, L.; Gobrecht, D. Evolution, Nucleosynthesis, and Yields of AGB Stars at Different Metallicities. III. Intermediate-mass Models, Revised Low-mass Models, and the ph-FRUITY Interface. *ApJS* **2015**, *219*, 40. [CrossRef]
9. Straniero, O.; Cristallo, S.; Piersanti, L. Heavy elements in globular clusters: the role of asymptotic giant branch stars. *ApJ* **2014**, *785*, 77. [CrossRef]
10. Young, P.A. Stellar Hydrodynamics in Radiative Regions. *ApJ* **2003**, *595*, 1114. [CrossRef]
11. Roederer, I.U. Characterizing the heavy elements in globular cluster M22 and an empirical s-process abundance distribution derived from the two stella groups. *ApJ* **2011**, *742*, 37. [CrossRef]
12. Terlizzi, R.; Abbondanno, U.; Aerts, G.; Alvarez, H.; Alvarez-Velarde, F.; Andriamonje, S.; Andrzejewski, J.; Assimakopoulos, P.; Audouin, L.; Badurek, G.; et al. The $^{139}La(n,\gamma)$ cross-section: Key for the onset of the s-process. *Phys. Rev. C* **2007**, *75*, 035807. [CrossRef]
13. Dillmann, I.; Plag, R.; Käppeler, F.; Rauscher, T. KADoNiS v0.3—The third update of the "Karlsruhe Astrophysical Database of Nucleosynthesis in Stars". In Proceedings of the Workshop "EFNUDAT Fast Neutrons—Scientific Workshop on Neutron Measurements, Theory & Applications", Geel, Belgium, 28–30 April 2009.
14. Käppeler, F.; Toukan, K.A.; Schumann, M.; Mengoni, A. Neutron capture cross-sections of the cerium isotopes for s- and p-process studies. *Phys. Rev. C* **1996**, *53*, 1397–1408. [CrossRef]
15. de L. Musgrove, A.R. Resonance Neutron Capture in ^{138}Ba and ^{140}Ce and the Prompt Neutron Correction to γ-ray Detectors. *Aust. J. Phys.* **1979**, *32*, 213–221.
16. Koehler, P.E.; Winters, R.R.; Guber, K.H.; Rauscher, T.; Harvey, J.A.; Raman, S.; Spencer, R.R.; Blackmon, J.C.; Larson, D.C.; Bardayan, D.W.; et al. High-resolution neutron capture and transmission measurements, and the stellar neutron-capture cross-section of ^{88}Sr. *Phys. Rev. C* **2000**, *62*, 055803. [CrossRef]
17. Brown, D.A.; Chadwick, M.B.; Capote, R.; Kahler, A.C.; Trkov, A.; Herman, M.W.; Sonzogni, A.A.; Danon, Y.; Carlson, A.D.; Dunn, M.; et al. ENDF/B-VIII: The 8*th* Major Release of the Nuclear Reaction Data Library with CIELO-project Cross Sections, New Standards and Thermal Scattering Data. *J. Nucl. Data Sheets* **2018**, *148*, 1–142. [CrossRef]
18. Shibata, K.; Iwamoto, O.; Nakagawa, T.; Iwamoto, N.; Ichihara, A.; Kunieda, S.; Chiba, S.; Furutaka, K.; Otuka, N.; Ohsawa, T.; et al. JENDL-4.0: A New Library for Nuclear Science and Engineering. *J. Nucl. Sci. Technol.* **2011**, *48*, 0022–3131. [CrossRef]
19. Plompen, A.J.M.; Cabellos, O.; De Saint, J.C.; Fleming, M.; Algora, A.; Angelone, M.; Archier, P.; Bauge, E.; Bersillon, O.; Blokhin, A.; et al. The joint evaluated fission and fusion nuclear data library, JEFF-3.3. *Eur. Phys. J. A* **2020**, *56*, 181. [CrossRef]
20. Dillmann, I.; Heil, M.; Käppeler, F.; Plag, R.; Rauscher, T.; Thielemann, F.K. The Karlsruhe Astrophysical Database of Nucleosynthesis in Stars 1.0 (test version). *Am. Inst. Phys. Conf. Ser.* **2006**, *819*, 123.
21. n_TOF Collaboration Website. Available online: https://ntof-exp.web.cern.ch/ (accessed on 15 February 2021).
22. Mazzone, A.; Cristallo, S.; Aberle, O.; Alaerts, G.; Alcayne, V.; Amaducci, S.; Andrzejewski, J.; Audouin, L.; Babiano-Suarez, V.; Bacak, M.; et al. Measurement of the $^{154}Gd(n,\gamma)$ cross-section and its astrophysical implications. *Phys. Lett. B* **2020**, *804*, 135405. [CrossRef]
23. Rukelj, Z.; Homes, C.C.; Orlita, M.; Akrap, A. Neutron Capture on the s-Process Branching Point ^{171}Tm via Time-of-Flight and Activation. *Phys. Rev. Lett.* **2020**, *125*, 142701.
24. Guerrero, C.; Tsinganis, A.; Berthoumieux, E.; Barbagallo, M.; Belloni, F.; Gunsing, F.; Weiß, C.; Chiaveri, E.; Calviani, M.; Vlachoudis, V.; et al. Performance of the neutron time-of-flight facility n_TOF at CERN. *Eur. Phys. J. A* **2013**, *49*, 27. [CrossRef]
25. Plag, R.; Heil, M.; Käppeler, F.; Pavlopoulos, P.; Reifarth, R.; Wisshak, K.; n_TOF Collaboration. An optimized C_6D_6 detector for studies of resonance-dominated (n,γ) cross-sections. *Nucl. Instrum. Methods Phys. Res. A* **2003**, *496*, 425–436. [CrossRef]

26. Marrone, S.; Mastinu, P.F.; Abbondanno, U.; Baccomi, R.; Marchi, E.B.; Bustreo, N.; Colonna, N.; Gramegna, F.; Loriggiola, M.; Marigo, S.; et al. A low background neutron flux monitor for the n_TOF facility at CERN. *Nucl. Instrum. Methods Phys. Res. A* **2004**, *517*, 389–398. [CrossRef]
27. Macklin, R.L.; Gibbons, J.H. Capture-Cross-section Studies for 30-220-keV Neutrons Using a New Technique. *Phys. Rev.* **1967**, *159*, 1007–1012. [CrossRef]
28. Schillebeeckx, P.; Becker, B.; Danon, Y.; Guber, K.; Harada, H.; Heyse, J.; Junghans, A.R.; Kopecky, S.; Massimi, C.; Moxon, M.C.; et al. Determination of Resonance Parameters and their Covariances from Neutron Induced Reaction Cross Section Data. *Nucl. Data Sheets* **2012**, *113*, 3054–3100. [CrossRef]
29. Agostinelli, S.; Allison, J.; Amako, K.A.; Apostolakis, J.; Araujo, H.; Arce, P.; Asai, M.; Axen, D.; Banerjee, S.; Barrand, G.; et al. Geant4–a simulation toolkit. *Nucl. Instrum. Methods Phys. Res. A* **2003**, *506*, 250–303. [CrossRef]
30. Barbagallo, M.; Guerrero, C.; Tsinganis, A.; Tarrio, D.; Altstadt, S.; Andriamonje, S.; Andrzejewski, J.; Audouin, L.; Bécares, V.; Bečvář, F.; et al. High-accuracy determination of the neutron flux at n_TOF. *Eur. Phys. J. A* **2013**, *49*, 156. [CrossRef]
31. Macklin, R.L.; Halperin, J.; Winters, R.R. Absolute neutron capture yield calibration. *Nucl. Instrum. Methods Phys. Res. A* **1979**, *164*, 213–214. [CrossRef]
32. Larson, N. *Updated Users' Guide for SAMMY Multilevel R-Matrix Fits to Neutron Data Using Bayes' Equation*; Tech. Rep. ORNL/TM-9179/R4; Oak Ridge National Laboratory: Oak Ridge, TN, USA, 1998.